OLD DOMINION UNIVERSITY RESEARCH FOUNDATION

DEPARTMENT OF MECHANICAL ENGINEERING AND MECHANCIS
SCHOOL OF ENGINEERING
OLD DOMINION UNIVERSITY
NORFOLK, VIRGINIA

EXPERIMENTAL STUDIES ON THE EFFECTS OF A STING SUPPORT ON THE PRESSURE DISTRIBUTION AROUND A SPHERICAL OBJECT

By

P.S. Barna

Progress Report
For the period August 1977 to August 1978

Prepared for the
National Aeronautics and Space Administration
Langley Research Center
Hampton, Virginia

Under
Research Grant NSG 1143
David D. Kershner, Technical Monitor
Flight Electronics Division

February 1979

TABLE OF CONTENTS

LIST OF TABLES

LIST OF FIGURES

(Continued)

LIST OF FIGURES (Concluded)

EXPERIMENTAL STUDIES ON THE EFFECTS OF A STING SUPPORT ON THE PRESSURE DISTRIBUTION AROUND A SPHERICAL OBJECT

By

P.S. Barna[1]

SUMMARY

Experiments were conducted on a spherical object, 2.5 inches in diameter, to obtain the pressure distribution around its meridian plane (containing the largest circle). In most of the tests the sphere was provided with a "tail"[2] consisting of a circular cylinder that was attached directly to the rear with its axis in alignment with the center of the sphere. In some tests the tail was removed and the sphere alone was tested for comparison purposes. The main object of the tests was to obtain information on tail interference with the pressure distribution.

From the measured pressure distribution certain predictions on the performance of the sphere can be made when it is employed as a sensor "head." Such a sensor is currently under investigation for employment as a flow indicator both for magnitude and direction.

The results of the tests show that the pressure distribution was affected by the presence of the tail to a minor extent only, while major differences occurred with the variation of the Reynolds number.

The experiments were performed both in an open as well as inside a closed wind tunnel under steady flow conditions at Reynolds numbers ranging from 0.91 to 2.6×10^5. Both wind tunnels are located in the Engineering Laboratories of Old Dominion University.

---

[1] Research Professor, Department of Mechanical Engineering and Mechanics, Old Dominion University, Norfolk, Virginia 23508.

[2] The tail may be considered as a model of a sting support widely employed in wind tunnels and aircraft installations to hold an object from the rear.

INTRODUCTION

When a sensor head of spherical shape is employed for flow measurements, usually three ports[3] are employed, one port being in the center while the other two are the side ports located at equal distances on either side of the center port. Facing the stream, the center port senses the stagnation while the side ports sense the static pressure. If the ports are differentially connected to manometers, the center and one of the side ports can be used to measure velocity, while the pressure differential between side ports can measure flow direction.

In employing a spherical head as a flow sensor, the problem of supporting the head arises. For this, normally a "sting"[4] is attached to the rear of the sphere diagonally opposite the center port. Under steady flow conditions the dimension of the sting may be small compared with the size of the sphere and therefore its interference with the flow may be so small that it can be ignored. There are, however, possible applications when the sting needs to be larger, and thus its dimension may become close or even equal to the diameter of the sphere. Such applications arise when the sensor is attached to a dynamic system, like a helicopter blade, in which case the ports sensing pressure are connected to pressure transducers housed inside the sphere. In such a case the support must be adequately strong and rigid to withstand severe accelerations and vibrations, and its interference with the flow may not be ignored.

Earlier investigations (ref. 1) of sting interference with pressure distribution show the effects of sting size (represented by the sting diameter). By directly measuring the drag force on the sphere, it was found that increasing the size of the sting results in a decrease in drag because of the streamlining effect of the "afterbody." It appears that a marked decrease in drag was experienced at Reynolds numbers greater than about 3×10^5. It was also found that the turbulence level in the stream strongly affects transition from laminar boundary layer flow to turbulent flow.

---

[3] The ports referred to are holes drilled into the surface.

[4] The "sting" is employed for support. The "tail" is employed to simulate the effect of sting on the flow.

While data on pressure distribution on isolated spheres can be found (ref. 2), a lack of data exists if a tail is attached. To fill this gap, experiments were planned to first investigate the effects of the tail on pressure distribution and compare this with the isolated sphere. Subsequently, the data were applied to establish the relation between incidence and pressure differentials between the various ports.

Sensors with spherical head configurations have been extensively used as yawmeters. In this application the general procedure is to turn the head until the center port faces the fluid stream and the pressure difference between the side ports reduces to zero. In two-dimensional flow, one pair of side ports suffices, while in three-dimensional flow two pairs are required. Each pair of side or static ports lies in the meridian plane at rectangles, while the central stagnation port is located in the center. In this application the size of sting has no significance.

In a more specialized application, when the spherical head is fixed to a rigid structure and cannot be turned into the stream, the center port can only sense stagnation if the stream happens to flow in the direction of the axis of symmetry. However, generally the flow would meet the sensor at an incidence, that is at some angle enclosed between the flow direction and the axis of symmetry. It may be anticipated that there would be a limit to the acceptance of all flow directions, and experience shows that this maximum limiting incidence angle must be determined from experiments. It is certain that the general performance, including the acceptance angle, must depend on the position of the side ports relative to the center port, which is usually given as the angle enclosed between the radii drawn to the ports from the sphere's center. From a theoretical viewpoint, it is convenient to use 45 degrees so that the angle enclosed between the side ports then becomes 90 degrees. Other considerations make one believe that the Reynolds number can have an effect in determining the optimum position of the side ports.

THEORETICAL CONSIDERATIONS

Based on potential flow theory (ref. 3), the pressure coefficient C_p around the meridian circle of a spherical object varies as

$$C_p = 1 - b_o \sin^2 \theta_i \tag{1}$$

where θ_i is the spherical angle enclosed between the stagnation point S and a static "port" i located at the θ_i angle on the surface as shown in figure 1. The theory predicts the exact value of the constant as being $b_o = 9/4 = 2.25$.

The theory may be applied to establish the pressure difference between ports located on the surface. We are especially interested in establishing the pressure difference between three ports of which port 1 lies in the line of symmetry, halfway between "side" ports 2 and 3 as shown in figure 2. Since by definition

$$C_p = \frac{\Delta p}{\frac{1}{2}\rho U^2}$$

the difference in pressure between ports 1 and 2 may be written

$$\Delta C_{p12} = \frac{\Delta p_{12}}{q} = \frac{p_1 - p_2}{\frac{1}{2}\rho U^2} = b_o(\sin^2 \theta_2 - \sin^2 \theta_1) \tag{2}$$

Similarly, the pressure difference between ports 2 and 3 becomes

$$\Delta C_{p23} = \frac{\Delta p_{23}}{q} = \frac{p_2 - p_3}{\frac{1}{2}\rho U^2} = b_o(\sin^2 \theta_3 - \sin^2 \theta_2) \tag{3}$$

If the flow approaches the sphere at an angle θ enclosed between the flow direction and the line of symmetry, the pressure differences in equations (2) and (3) can be expressed in terms of θ provided the angles θ_2 and θ_3 are specified.

Employ the identity

$$\sin^2 \theta_3 - \sin^2 \theta_2 = \sin(\theta_3 + \theta_2) \sin(\theta_3 + \theta_2)$$

and select the angle enclosed between ports 2 and 3 to be exactly 90 degrees, so that $\theta_2 + \theta_3 = \pi/2$. If the flow approaches the sphere at the angle θ,

the stagnation point moves from 1 to S; then $\theta_2 = \pi/4 - \theta$ and $\theta_3 = \pi/4 + \theta$.

Hence $\theta_3 - \theta_2 = 2\theta$ and since $\theta_2 + \theta_3 = \pi/2$

$$\sin^2 \theta_3 - \sin^2 \theta_2 = \sin 2\theta$$

thus the pressure difference between the side ports becomes

$$\Delta C_{p23} = \frac{p_2 - p_3}{\frac{1}{2} \rho U^2} = b_o \sin 2\theta \tag{4}$$

Similarly, the identity

$$\sin^2 \theta_2 - \sin^2 \theta_1 = \sin(\theta_2 + \theta_1) \sin(\theta_2 - \theta_1)$$

and since $\theta_2 = \pi/4 - \theta$ and $\theta_1 - \theta$, one obtains

$$\sin^2 \theta_2 - \sin^2 \theta_1 = \frac{1}{\sqrt{2}} \sin \left(\frac{\pi}{4} - 2\theta \right)$$

and the pressure difference between center and side port 2 becomes

$$\Delta C_{p12} = \frac{p_1 - p_2}{\frac{1}{2} \rho U^2} = \frac{b_o}{\sqrt{2}} \sin \left(\frac{\pi}{4} - 2\theta \right) \tag{5}$$

For real, that is viscous flow, the sphere constant b_o may assume values that may differ from the 2.25 derived from potential flow theory. Thus we can anticipate a value b_{23} for ports 2 and 3 and a value b_{12} for ports 1 and 2. The real values of the sphere constant thus must be established from experiment.

EXPERIMENTAL APPARATUS AND METHOD OF TESTING

To obtain the pressure distribution, a spherical object of 2.5-inch diameter was placed into the airstream. The sphere was made of aluminum

and was supported by a horizontal hollow shaft press-fitted into the "side" of the sphere right up to its center. A single pressure tapping was radially drilled into the surface of the sphere at right angle to the axis of the hollow shaft, the hole also extending to center, as shown in figure 3. The shaft was set at right angle to the airstream, and, by rotating it about its axis, the pressure distribution around the sphere could be obtained. Since the diameter of the shaft was 0.375 inches, its interference with the airstream was considered minimal; however, it had to be reinforced for rigidity with a sleeve that extended through the tunnel walls. The sleeve fitted into the arbor extending from the turntable and was held in position by set screws. The angle of incidence was measured with a protractor provided with a Vernier scale so that the angle was measured with an accuracy of 0.1 degree.

The pressure experienced on the surface of the sphere propagated through the port to the center from where it was transmitted through the hollow shaft to a sensitive manometer. A pitot-static tube was employed near the sphere to measure the velocity of the stream and to provide the local pressure used as reference to the pressure on the sphere surface.

The experiments were first performed at the outlet of the open end wind tunnel and were subsequently repeated in the closed wind tunnel. The experimental setup in these tunnels is shown in figures 4 and 5.

Two types of experiments were performed. In the first type, the sphere alone was tested at various Reynolds numbers. In the second type of test, the sphere was provided with a "tail" consisting of a hollow circular cylinder located either diagonally opposite the center port or diagonally opposite the side ports.

Prior to each test the sphere was visually aligned so that the center hole faced the airstream. To check the accuracy of the visual alignment, the sphere was rotated to an angle, say 10 degrees, and pressure measurement was taken. Subsequently, it was rotated back into the opposite direction to -10 degrees and the pressure was again recorded. If the center was correctly aligned, the two pressure readings gave substantially the same result. An adjustment was made if the readings proved unequal, and the process was repeated until the desired result was obtained.

To study the effect of the tail, tests were performed with the tail located opposite the center port or opposite either of the two side ports.

This was easily achieved by drilling and tapping three holes exactly diagonally opposite the ports located at the face of the sphere. All tests performed with the 1.75-inch diameter tail were subsequently repeated with a 1.375-inch diameter tail (both tails were 6 inches long).

During each test the air velocity was kept constant and the incidence angle was varied by small steps, generally two to five degrees at a time. When the slope of the curves was steep, the increments were only one-half degree or less as required.

Air velocity was varied between 50 and 200 ft/s, that is, between the Reynolds number range 0.9 to 2.6 $\times$ 10^6.

All test runs were made with the sphere turning in one direction and were repeated in the opposite direction.

RESULTS

The results are presented in four sets of graphs. Figure 6 shows the conventional pressure distribution around 180 degrees of the isolated sphere, and the results are compared with the findings of another investigator. Figures 7 and 8 show results between ±75 degrees.

Figures 9 and 10 show the pressure distribution between angles ±75 degrees with the tail located diagonally opposite port 1 (center port) for both tails, 1.75-inch and 1.375-inch diameter respectively. Figures 11 and 12 show results of port 2, that is, when the tail was displaced by 45 degrees from the centerline. Figures 13 and 14 show results for port 3 similar to those obtained for port 2, except for the change in the sign of the angles. For both ports the measurements were taken between 105 and 20 degrees (for port 2 the range was -105 to +20 and for port 3, -20 to +105 degrees).

It appears from figures 6, 7, and 8 that pressure distribution is sensitive to Reynolds number effects and also to the level of turbulence present in the airstream (ref. 1). However, the magnitude of sensitivity also depends on incidence. Between 0 and 30 degrees the pressure coefficient falls from unity (1.0) to approximately 0.6 for all spheres tested, and in this range variation the pressure coefficient proves to be insensitive

to viscous effects. With increasing incidence, however, the sensitivity gradually increases and becomes greatest between 50 and 80 degrees. In further increasing the incidence, the sensitivity decreases again and becomes relatively small between 80 and 180 degrees. Furthermore, the sensitivity also manifests itself in a shift of the zero pressure[1], located at the intersection of the pressure distribution curve with the horizontal incidence. It was noticed that a marked change in the negative pressure peaks always occurred between 70 and 80 degrees. The shift in the zero pressure point may be observed from inspection of the graphs: at Re = 1.4×10^5 the intersection point is about ±45 degrees (fig. 7), while the point shifts to 43.6 degrees at Re = 2.6×10^5 as shown in figure 8.

The presence of the tail substantially lowered the value of $-C_p$min. With the 1.375-inch tail $C_p$min = -1.0 at Re = 0.91×10^5 (fig. 9a), while -1.15 is experienced at 1.4×10^5 (fig. 9b), and 1.23 at 2.6×10^5 (fig 9c). With increasing Reynolds number, zero first shifts from ±44.7 degrees (fig. 9a) to ±44.5 degrees (fig. 9b), then further decreases to about ±41 degrees at 2.6×10^5 (fig. 9c). Similar results were found with the 1.75-inch tail.

Experiments conducted at lower Reynolds numbers indicated some instability in the pressure which occurred at ±50 degrees when the 1.375-inch tail was attached. The manometer oscillated periodically and showed at one time a value of -0.2 and a moment or two later -0.3, and so two values appear for the same incidence in figures 9a and 9b. This instability was not observed in the closed tunnel at Re = 2.6×10^5. With the 1.75-inch tail, instability occurred around 52 degrees at low Reynolds numbers, but no instability was experienced at higher speeds (see figs. 9c and 10b).

Studies on port 2 are shown in figures 11 and 12, where the pressure distribution between angles of -105 and +20 degrees are presented. The resulting curves are superimposed for ready identification of the effects of Reynolds numbers ranging between 0.91 to 2.6×10^5. Peculiarities manifest themselves in the negative pressure range at lower Reynolds numbers; in addition to the shape changes of the curves, the shift in zero pressure angle, and the surges resulting from instability, there also

---

[1] Zero pressure is experienced when the difference between the free-stream pressure and surface pressure decreases to zero.

appears to be a break in the continuity around 45 degrees. This was observed only in the open tunnel. Once the Reynolds number attained a value of 2.4 to 2.6 $\times 10^5$, the pressure distribution curve became rather "regular," free of bumps and surges with the pressure coefficient attaining a minimum value of approximately -1.3 at -90 degrees. To facilitate interpretation of the results, the various positions of the tail—relative to the horizontal reference line—are also shown in figures 11 and 12. Similar results were obtained for port 3, as shown in figures 13 and 14.

The effects of both viscosity and turbulence level on transition from laminar to turbulent flow in the boundary layer are well known. It is therefore logical to assume that the zero pressure point is also affected by both. Because of the difference of turbulence level between the open and closed tunnels, separate experiments were conducted in the closed tunnel to study the effects of Reynolds number on the location of the zero pressure point. In other words, restricting tests to one tunnel eliminated the influence of turbulence level on transition by the other tunnel.

Results of these experiments are presented in figure 15 where the zero pressure incidence angle is plotted against Reynolds numbers between 0.55 and 2.6 $\times 10^5$. It appears that below Re = 1.2 $\times 10^5$ the changes are small. However, a sudden drop appears at 1.2 $\times 10^5$ followed by a gradual decrease with increasing Reynolds number. The curves flatten out after Re = 1.8 $\times 10^5$ and the zero point remains fixed at 41.5 degrees.

APPLICATION OF RESULTS

From the pressure distribution tests, the sphere constants b_{23} and b_{12} can be established. This entails the application of the results to a pair of ports, either 1 and 2 or 2 and 3, which need to be located at set angles. It may be convenient to assume 45 degrees as the set central angle between ports because then the central angle between ports 2 and 3 becomes a right angle. The procedure for obtaining the sphere constant was first to establish the angles enclosed by the portholes with the airstream when the sphere was set to an incidence θ. For example, when considering side ports 2 and 3, if θ = -20 degrees, then for port 3 the angle θ = +25 degrees and for port 2, θ = -65 degrees. Second, for these angles the pressure coefficient C_p was found from the experimental results. Thus at

Re = 2.6×10^5 the coefficients $C_{p2} = -0.85$ and $C_{p3} = +0.61$ were found. Their difference $\Delta C_{p23} = C_{p2} - C_{p3} = -1.46$. The procedure was repeated for incidence angles ranging from -30 to +30 degrees in convenient (5-degree) steps. For convenience, table 1 gives the values of θ_1, θ_2, and θ_3 at various incidences. Finally, the resulting ΔC_{p23} values were plotted against $\sin 2\theta$ for the side ports 2 and 3 as shown in figure 16, and ΔC_{p12} values were plotted against $\frac{1}{\sqrt{2}} \sin(45 - 2\theta)$ for the side ports 1 and 2, as shown in figure 17. The sphere constants were obtained from the slopes of the curves.

It appears from figure 16 that for side ports 2 and 3 and with the 1.75-inch tail, the sphere constant $b_{23} = 2.25$ at the high Reynolds number of 2.6×10^5, a result which completely agrees with the value of 2.25 predicted from potential flow theory. At the same Reynolds number, the center and side port constant $b_{12} = 2.23$, which is a value only 0.9 percent off 2.25. For lower Reynolds numbers, however, the sphere constants assume lesser values, depending on the Reynolds number, as shown in figures 16 and 17.

In the determination of the sphere constant b_{12}, only the linear portion of the curve was used. As it appears from figure 17, the top end of the curves turn around and form a loop, and the size of the loop seems to depend on the Reynolds number. It is noted that the function $\sin(45 - 2\theta)$ attains a maximum value of 1 when the angle $\theta = -22.5$ degrees, so the extreme of the horizontal abscissa ends at $\frac{1}{\sqrt{2}} = 0.707$. Since the experiments were conducted with angles up to 30 degrees, all angles below -22.5 degrees will cause the function $\sin(45 - 2\theta)$ to have values inboard of the extreme, hence b_{12} may not be considered constant below -22.5 degrees.

CONCLUSIONS

1. The results of the experiments show that the Reynolds number has a marked effect on the pressure distribution, while the presence of the tail, representing a sting support, has only a minor influence.

2. Reynolds number effects are manifested both in a shift in the location of zero pressure point experienced on the sphere's surface and in the shape of the distribution curves.

3. These effects ultimately influence the sphere constants b_{23} and b_{12} inasmuch as their values fall below the theoretically predicted value of 2.25 for the lower Reynolds numbers. However, for Re = 2.6×10^5, the experimentally obtained sphere constants appear to be remarkably close indeed to 2.25. Therefore, satisfactory data will result if probe operation is confined to Reynolds numbers of this value and greater.

4. The central angle of 45 degrees permits the sphere to be used as a probe for sensing flow direction within the range of +30 to -22.5 degrees.

5. Probes with central angles of less than 45 degrees can also be designed which would provide a larger angular range but with reduced output. The theoretical determination of the pressure coefficients would be more complicated.

REFERENCES

1. Hoerner, S.: Versuche mit Kugeln Betreffend Kennzahl, Turbulenz und Oberflachenbeschaffenheit. Luftfartforschung, vol. 12, no 1, 1935.

2. Fage, A.: Experiments on a Sphere at Critical Reynolds Numbers. Aero. Res. Council Reports and Memoranda No. 1766, 1936.

3. Yuan, S.W.: Foundations of Fluid Mechanics. Prentice-Hall, 1967, p. 235.

Table 1. Incidence angle of portholes (see fig. 2b).

Port 1 $\theta = \theta_1$ (degrees)	Port 2 $\theta = \theta_2$ (degrees)	Port 3 $\theta = \theta_3$ (degrees)
30	-15	75
25	-20	70
20	-25	65
15	-30	60
10	-35	55
5	-40	50
0	-45	45
-5	-50	40
-10	-55	35
-15	-60	30
-20	-65	25
-25	-70	20
-30	-75	15

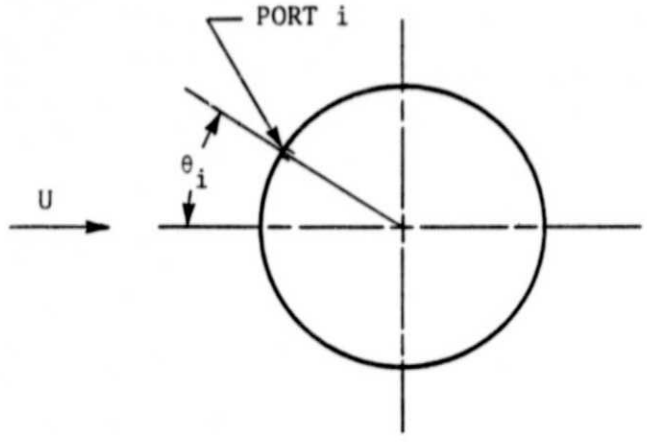

Figure 1. Spherical object provided with one port.

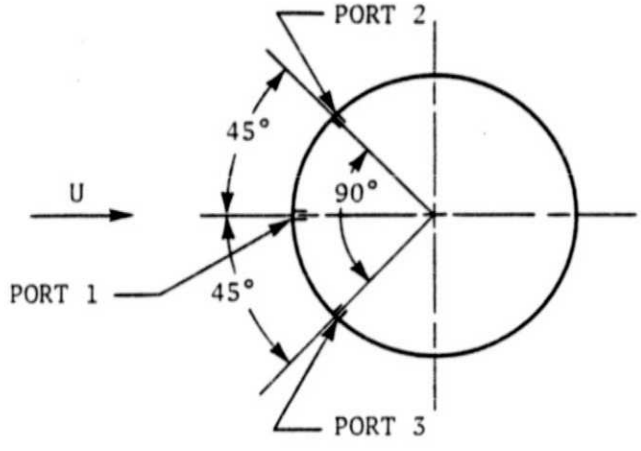

Figure 2(a). Spherical object provided with three ports; airflow at zero incidence.

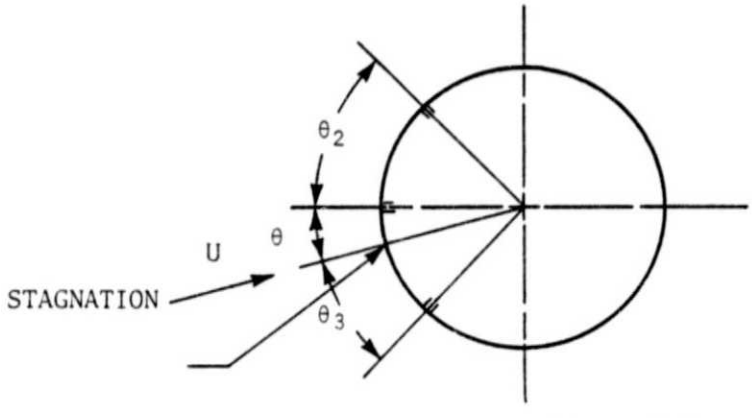

Figure 2(b). Spherical object with approaching airflow at incidence θ.

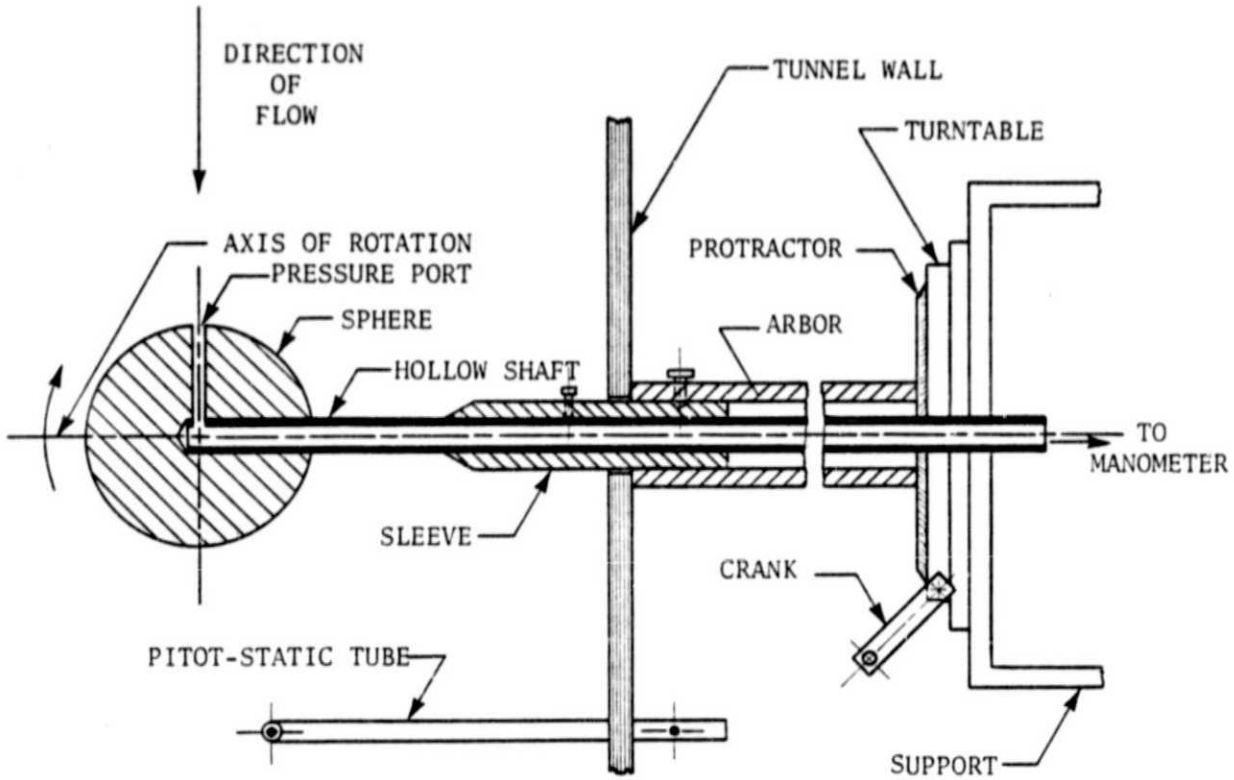

Figure 3. Schematic arrangement of sphere setup inside closed-circuit wind tunnel (not to scale).

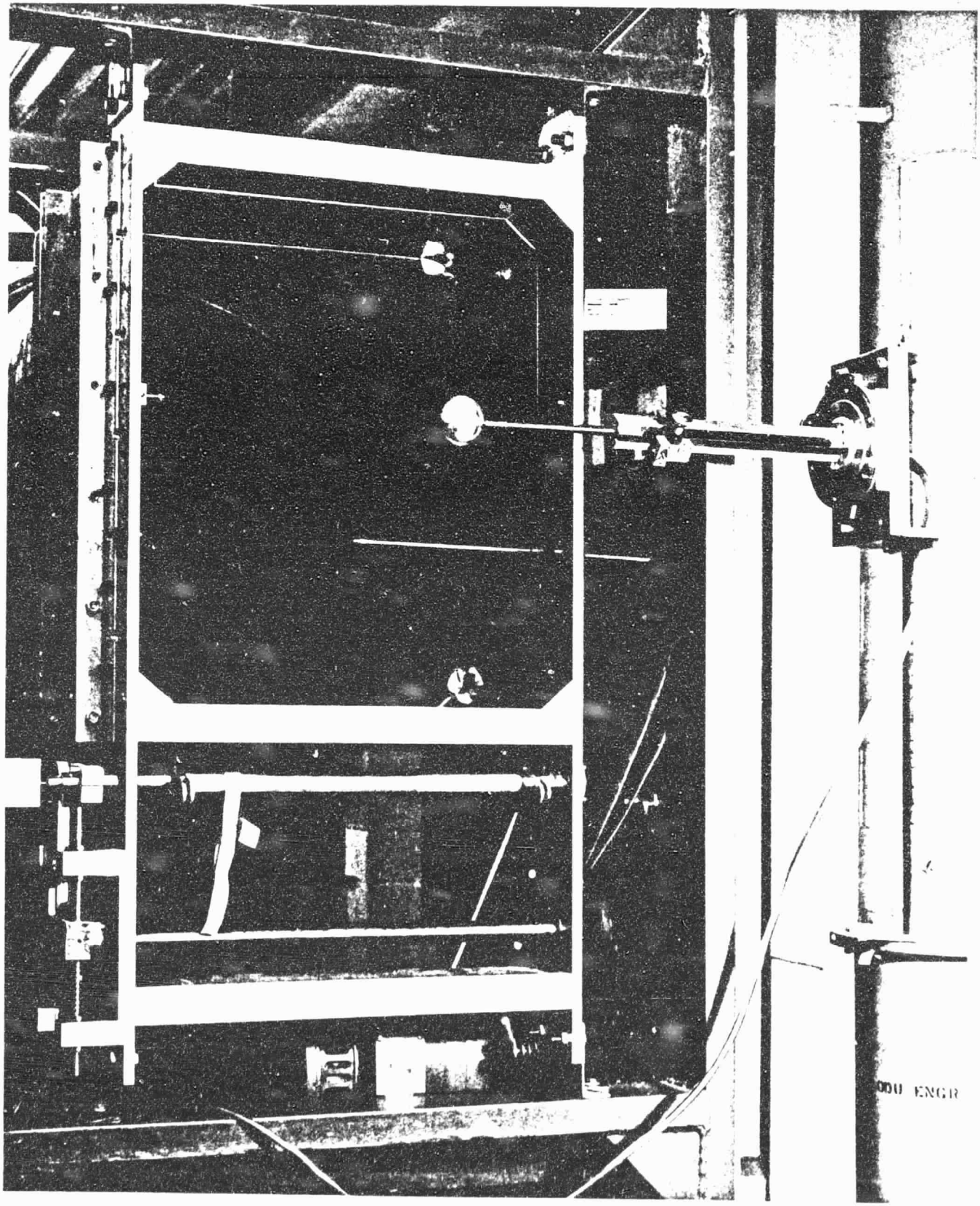

Figure 4. Experimental setup in the open wind tunnel (sphere without tail).

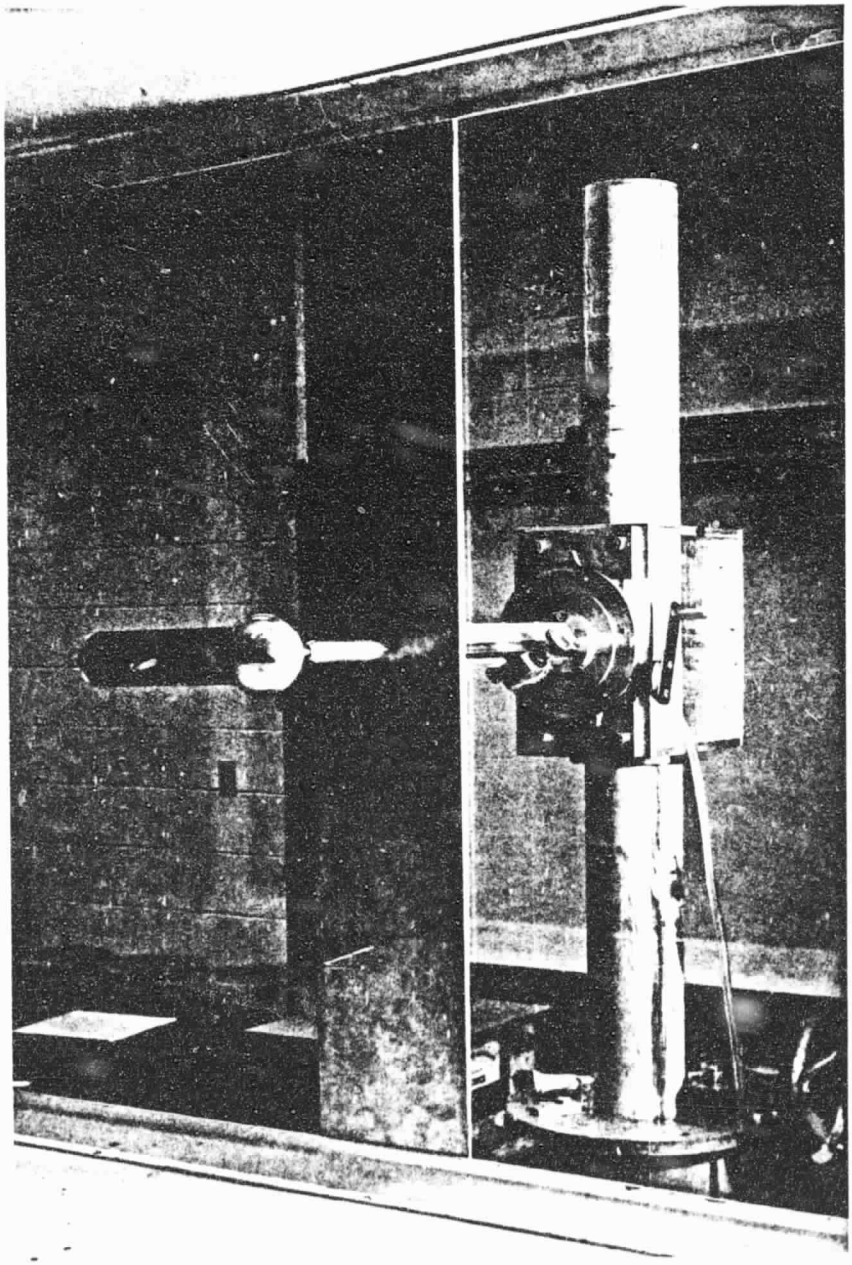

Figure 5. Experimental setup in the closed wind tunnel (sphere with tail).

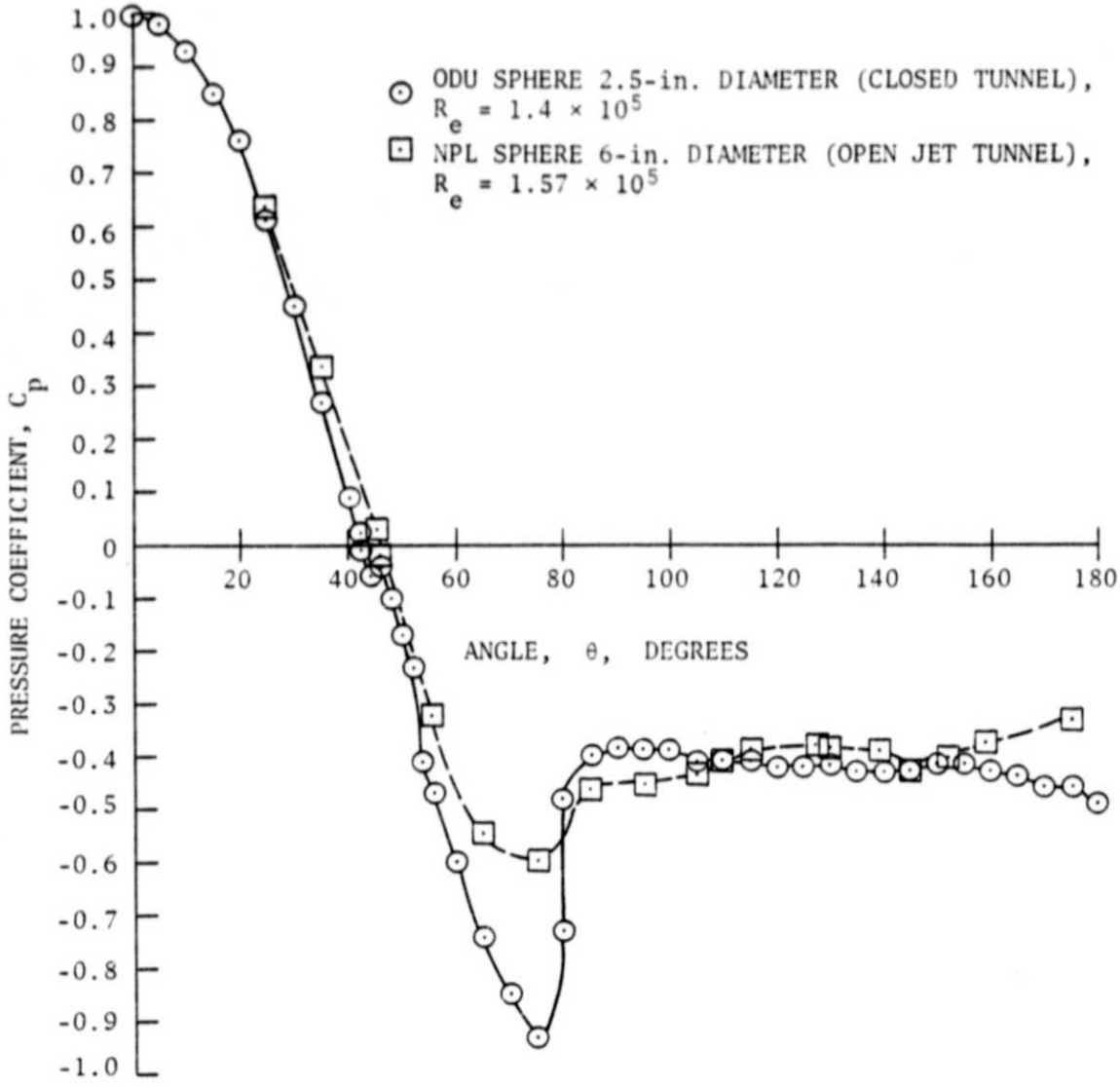

Figure 6. Comparison between the pressure distribution obtained at the ODU large wind tunnel and that obtained at NPL (England) at about the same Reynolds number.

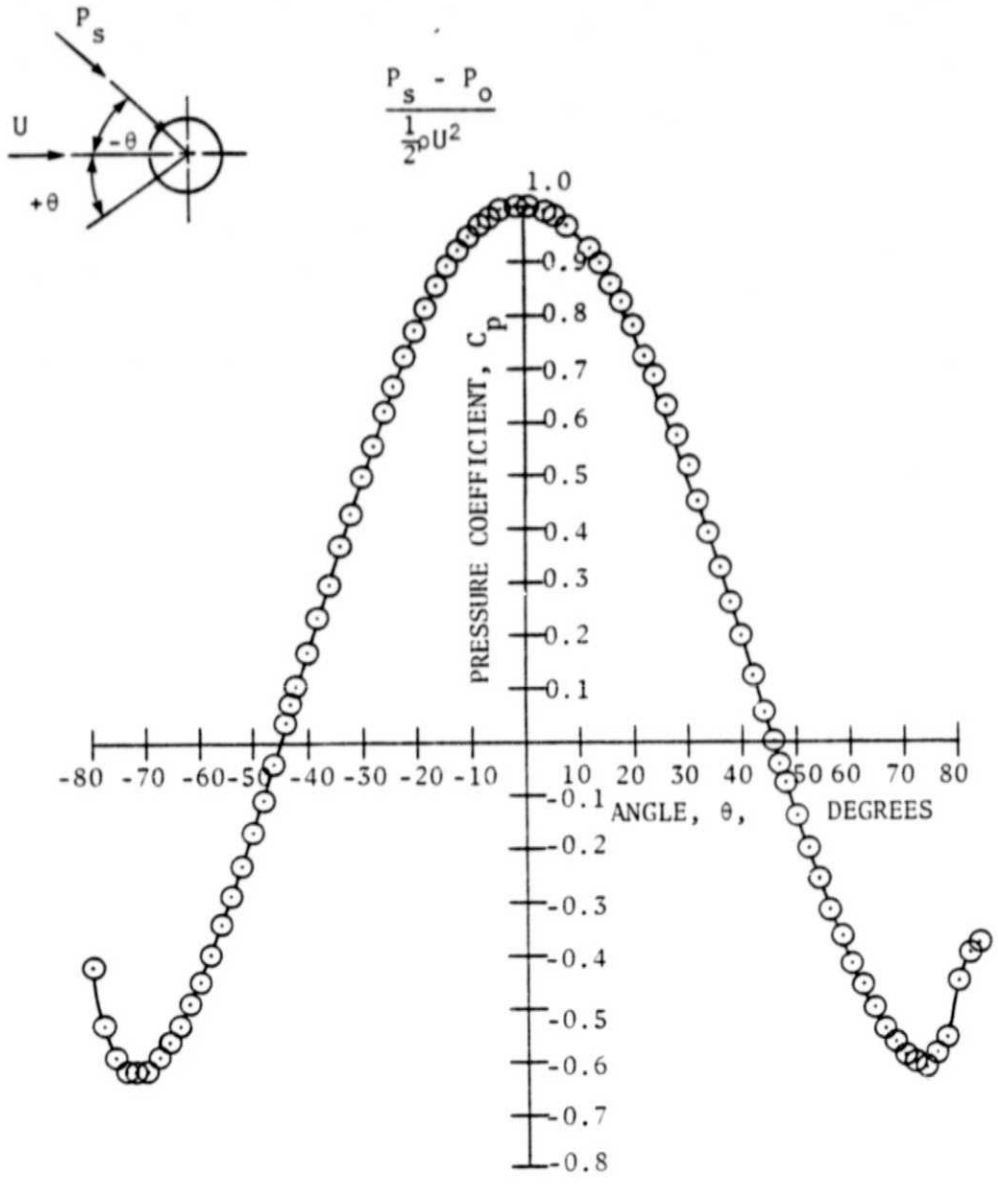

Figure 7. Pressure distribution around a 2.5-in. sphere without tail at $R_e = 1.4 \times 10^5$ obtained in the open wind tunnel.

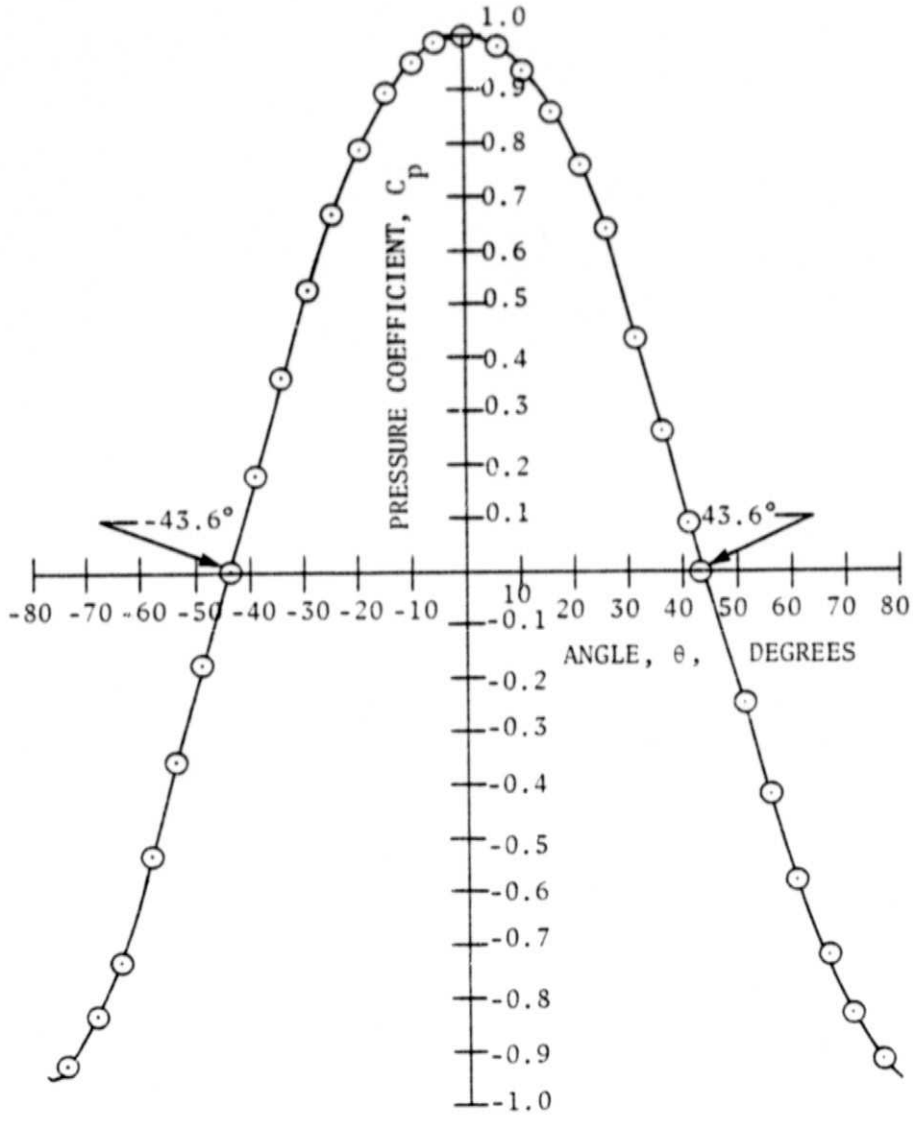

Figure 8. Pressure distribution around a 2.5-in. sphere without tail at $R_e = 2.6 \times 10^5$ obtained in the closed wind tunnel.

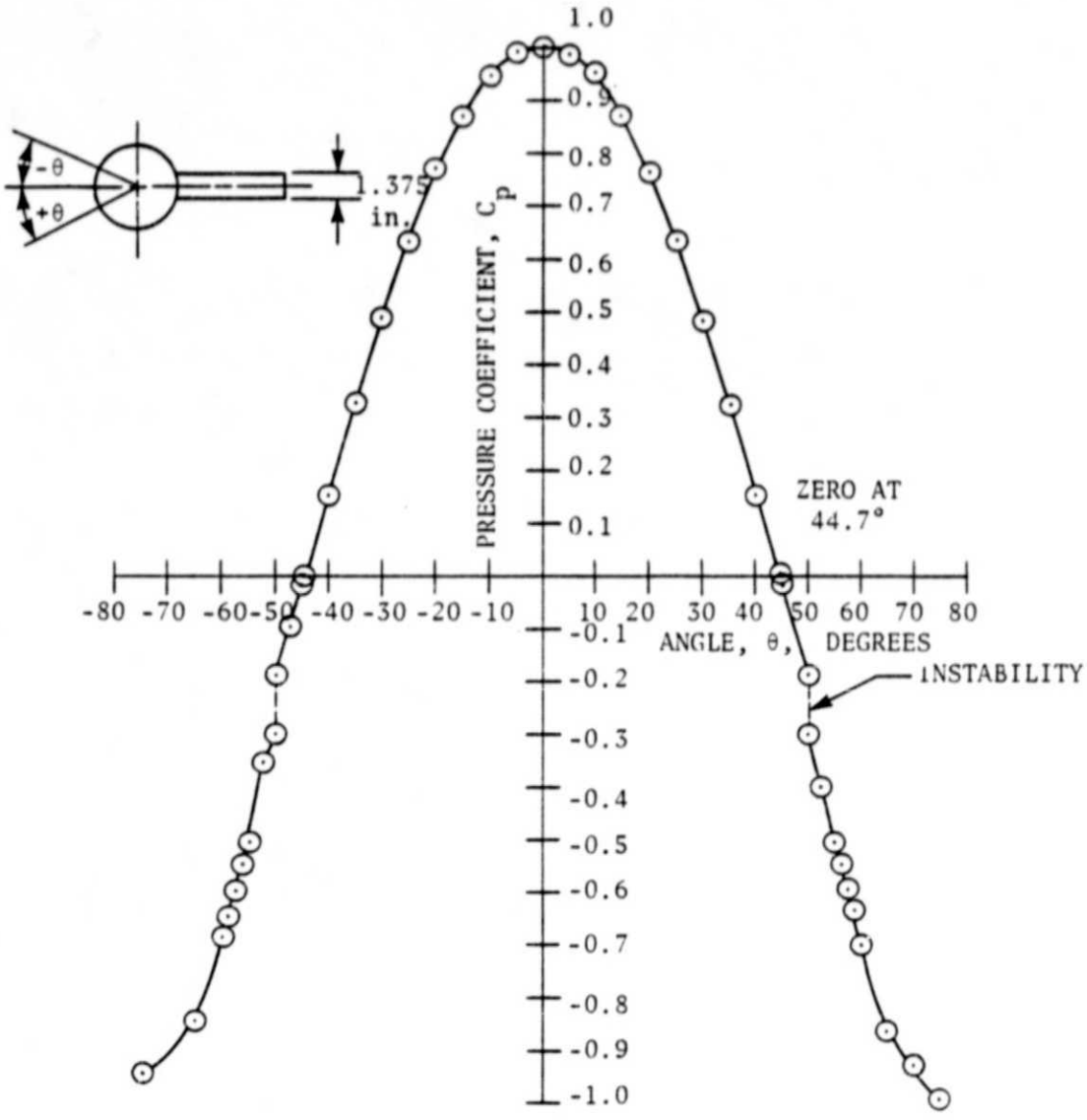

(a) $R_e = 0.91 \times 10^5$; open wind tunnel.

Figure 9. Pressure distribution around a 2.5-in. sphere fitted with a 1.375-in. tail.

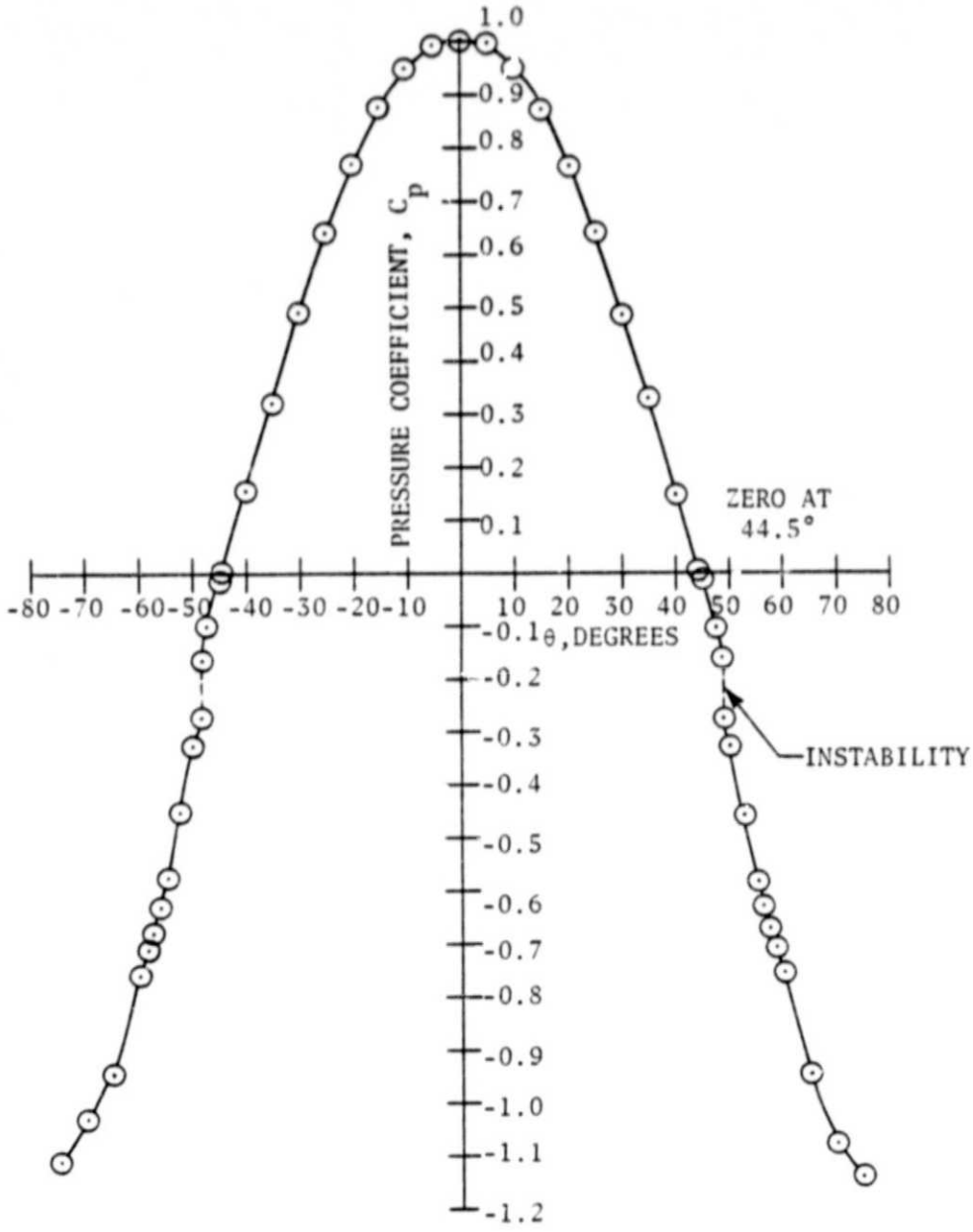

(b) $R_e = 1.4 \times 10^5$; open wind tunnel.

Figure 9. (Continued).

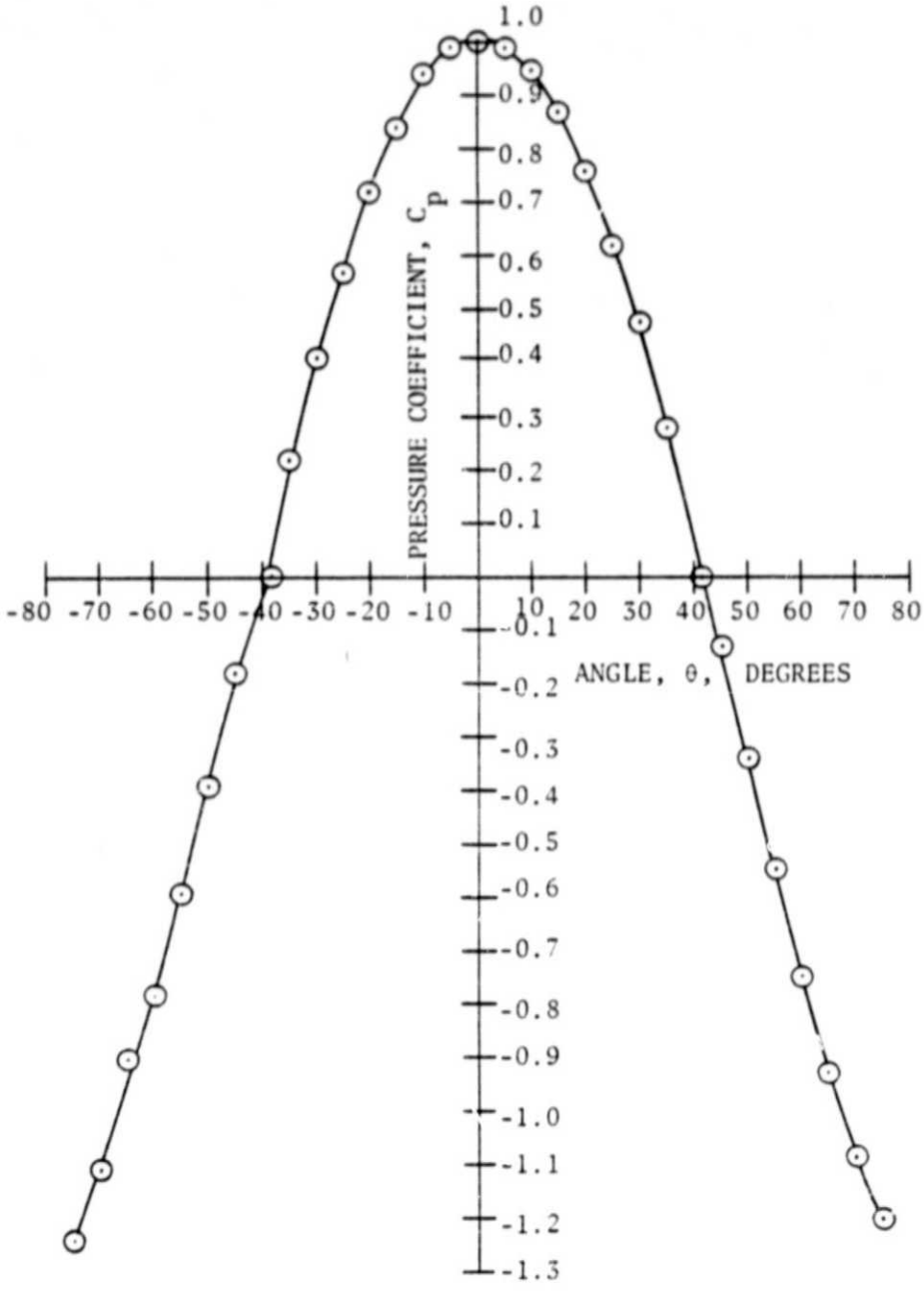

(c) $R_e = 2.6 \times 10^5$; closed wind tunnel.

Figure 9. (Concluded).

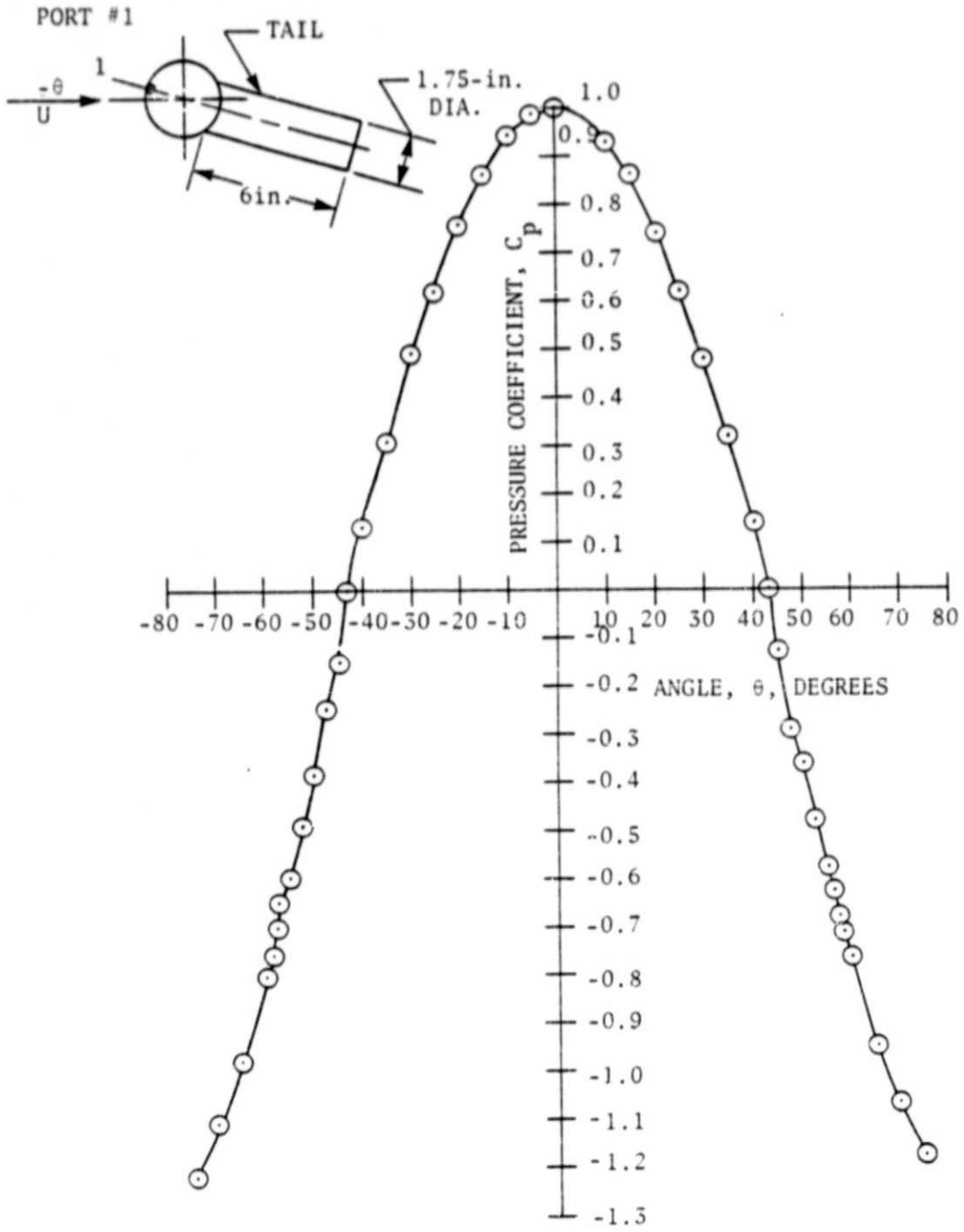

(a) $R_e = 0.91 \times 10^5$; closed wind tunnel.

Figure 10. Pressure distribution around a 2.5-in. sphere fitted with a 1.75-in. tail.

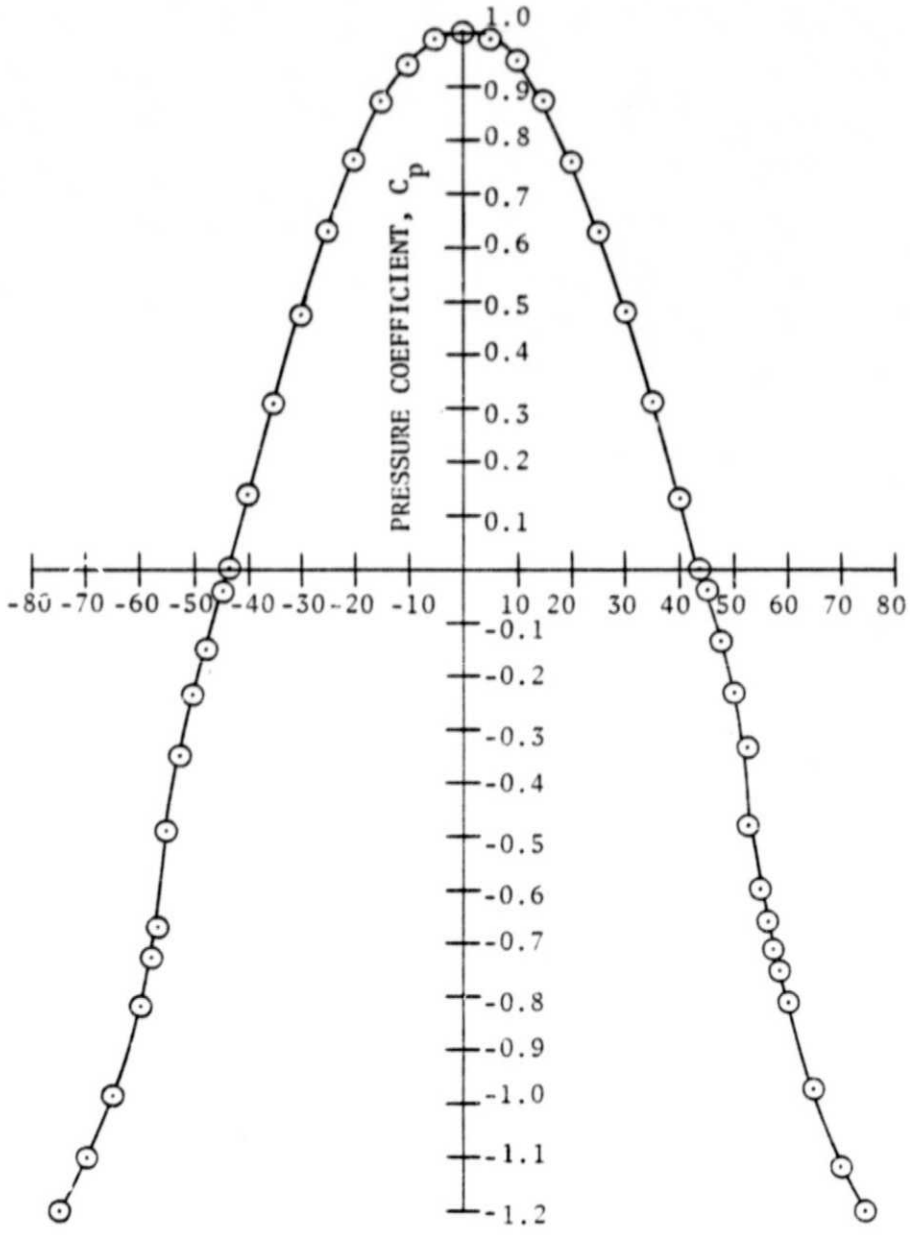

(b) $R_e = 1.4 \times 10^5$; open wind tunnel.

Figure 10. (Continued).

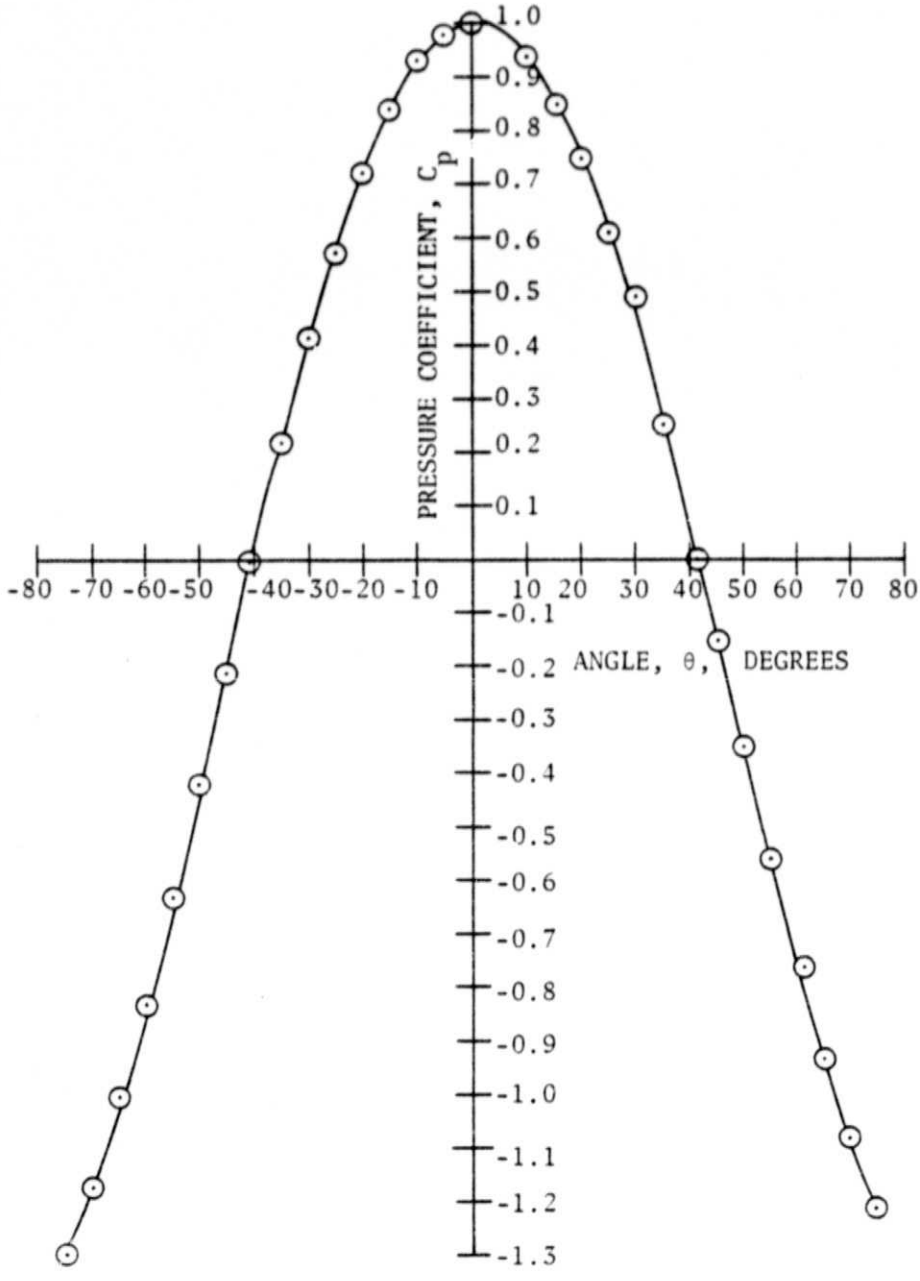

(c) $R_e = 2.6 \times 10^5$; closed wind tunnel.

Figure 10. (Concluded).

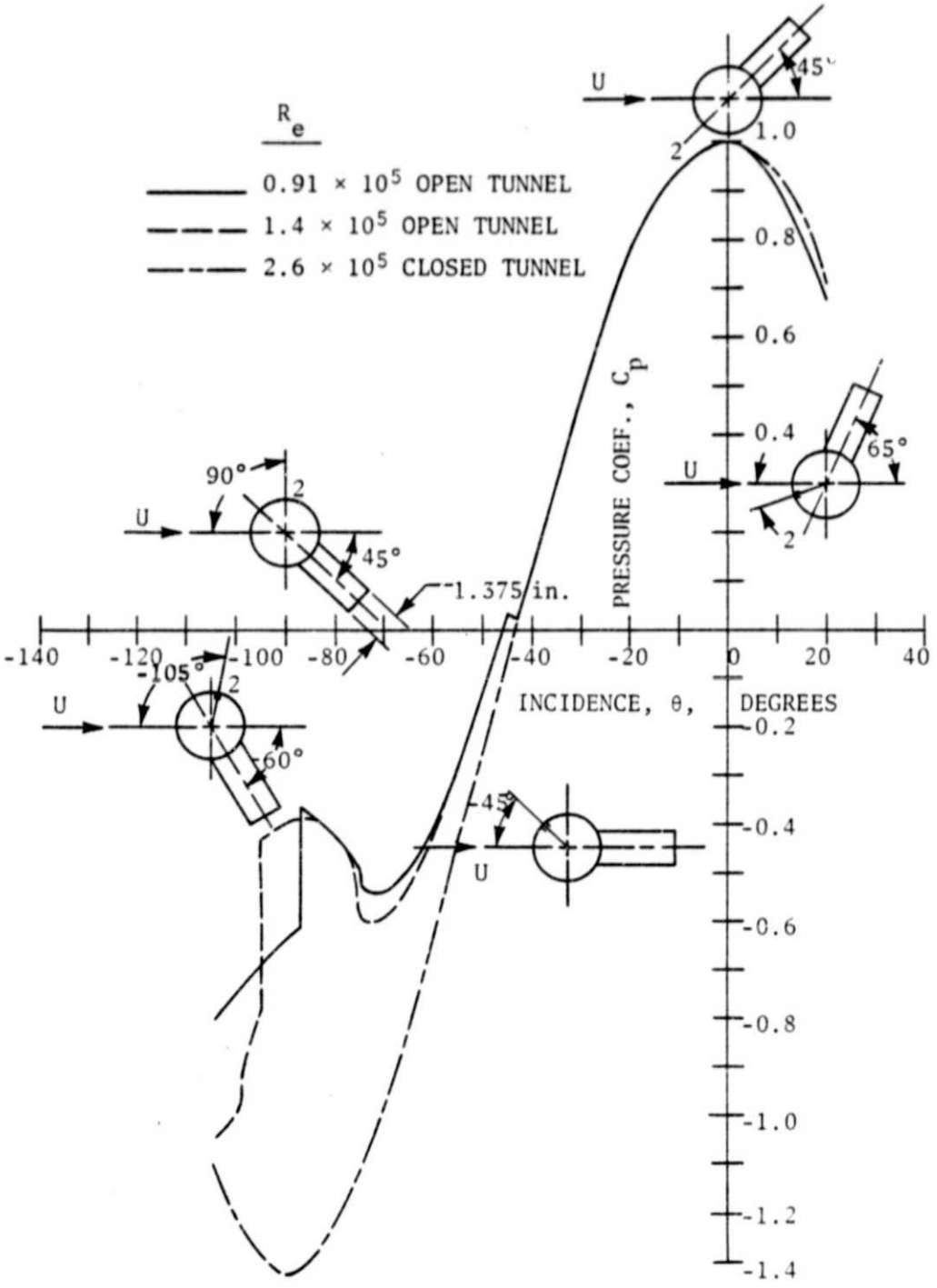

Figure 11. Pressure distribution around a 2.5-in. sphere fitted with a 1.375-in. tail, port 2.

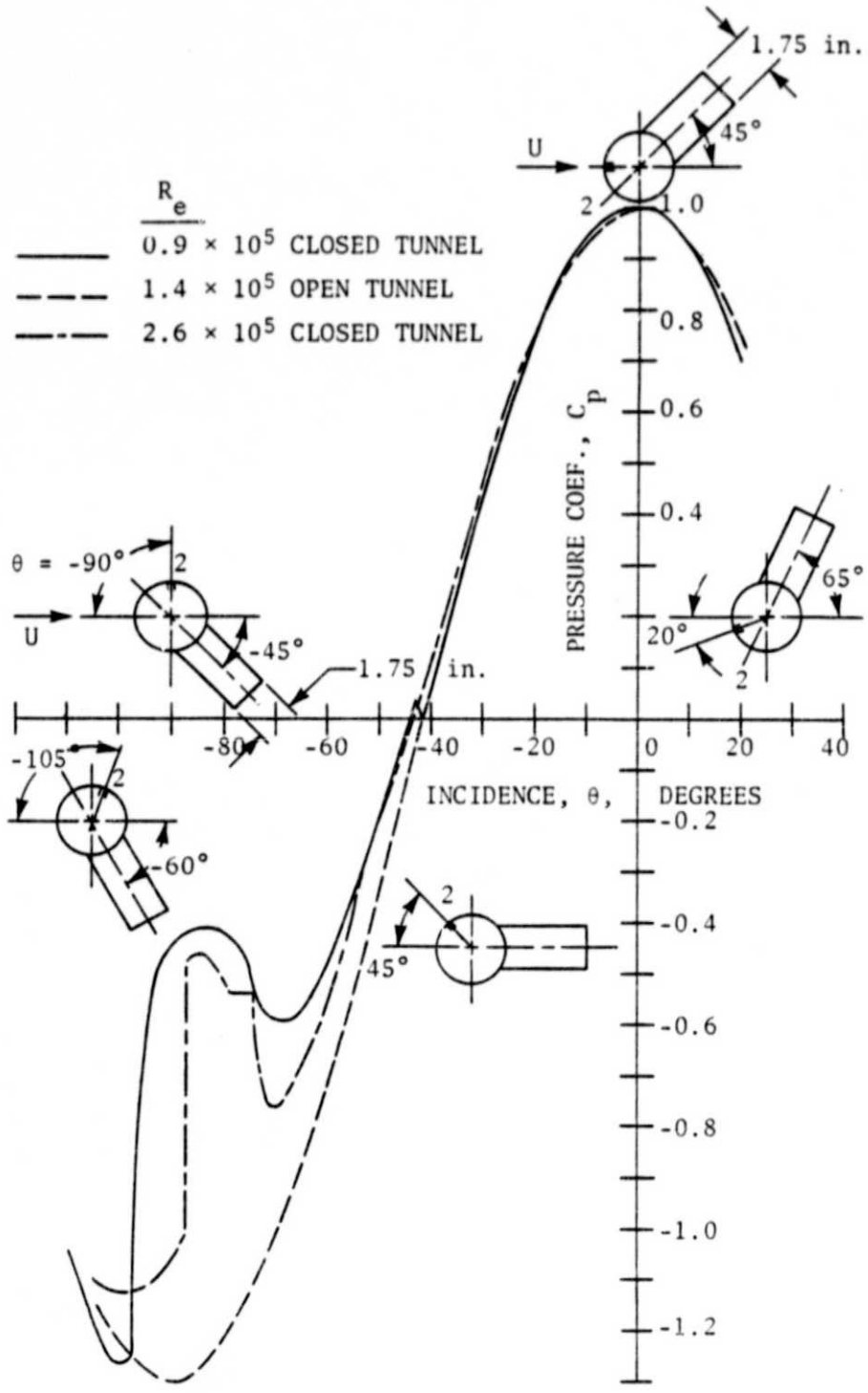

Figure 12. Pressure distribution around a 2.5-in. sphere fitted with a 1.75-in. tail, port 2.

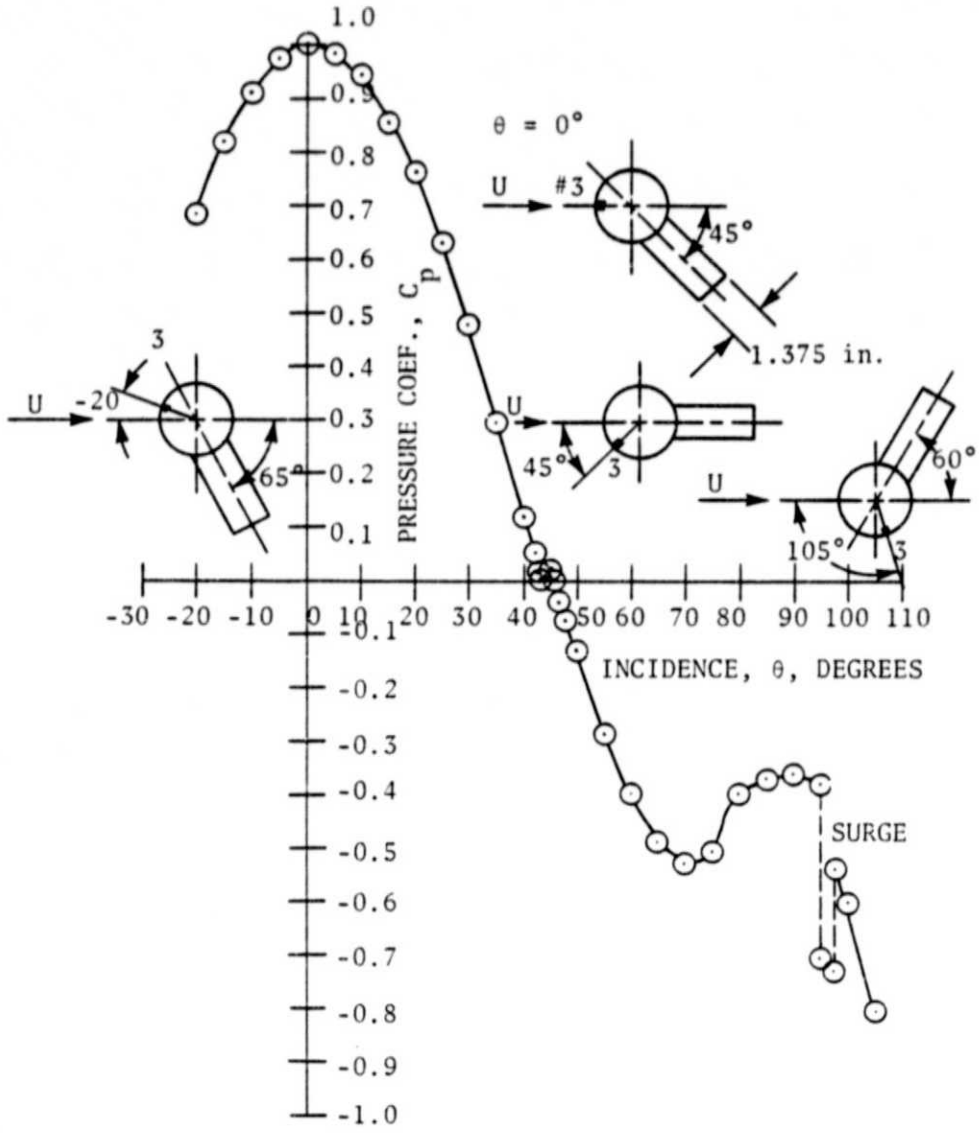

(a) $R_e = 0.91 \times 10^5$; open wind tunnel.

Figure 13. Pressure distribution around a 2.5-in. sphere fitted with a 1.375-in. tail, port 3.

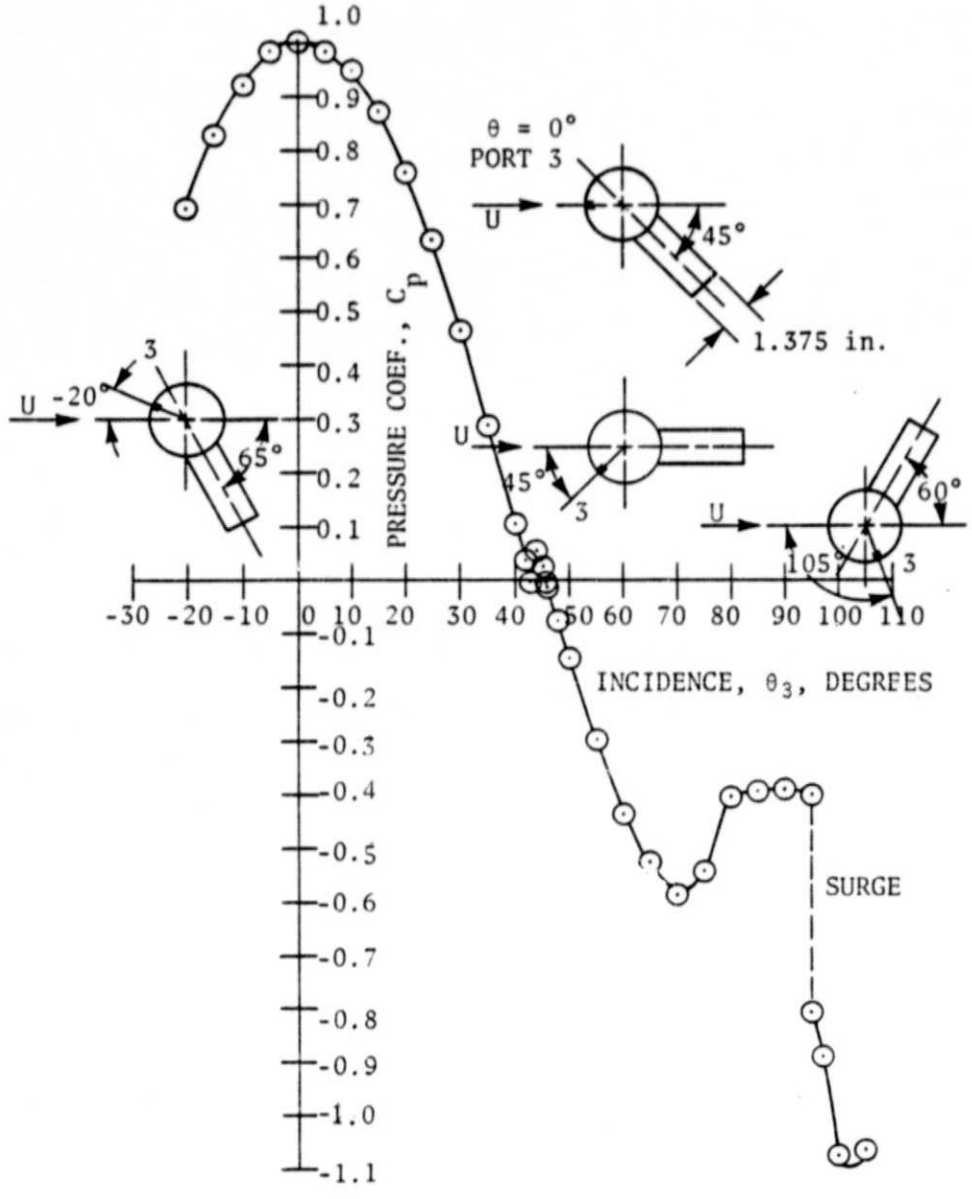

(b) $R_e = 1.4 \times 10^5$; open wind tunnel.

Figure 13. (Concluded).

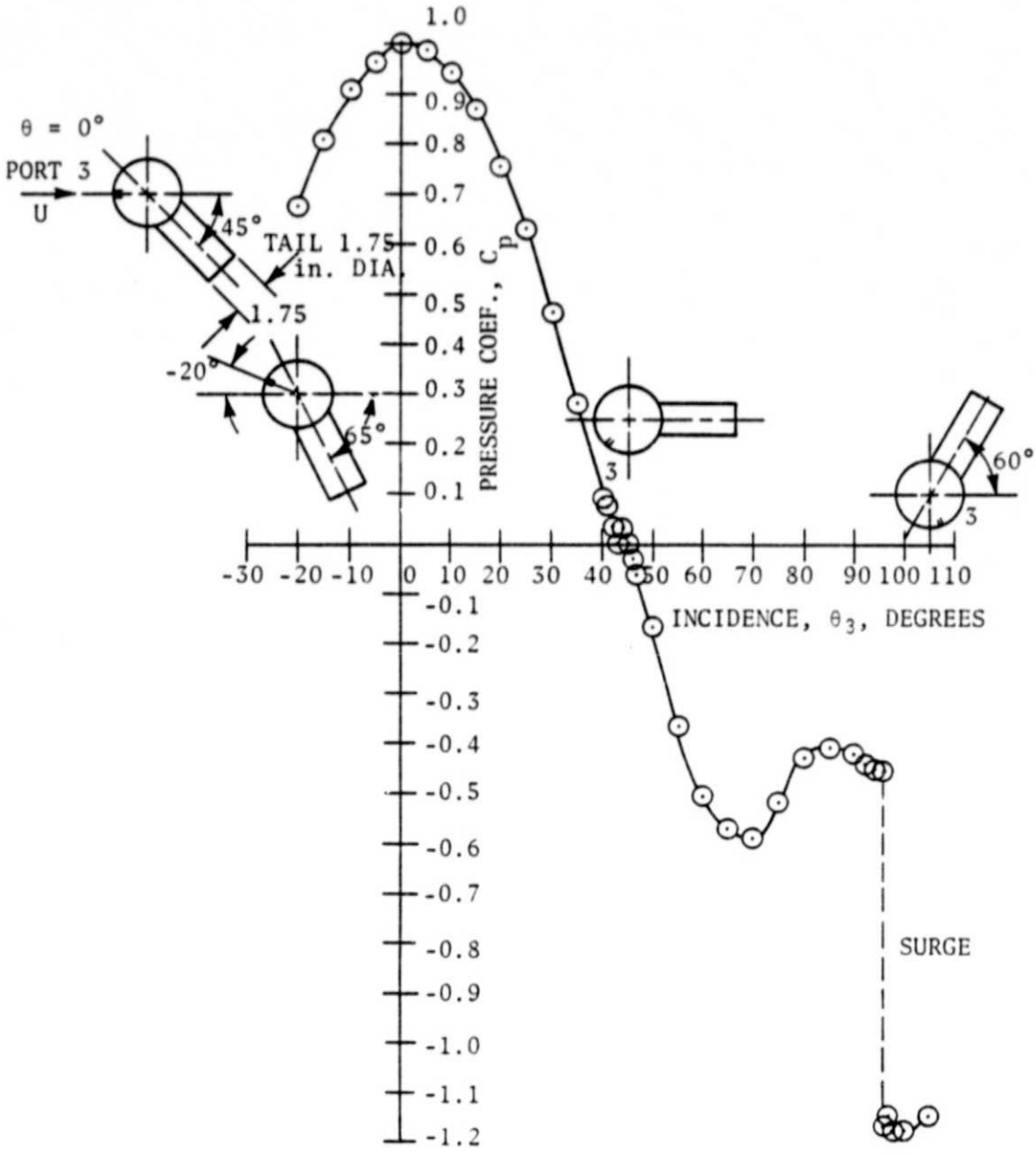

Figure 14. Pressure distribution around a 2.5-in. sphere fitted with a 1.75-in. tail, port 3.

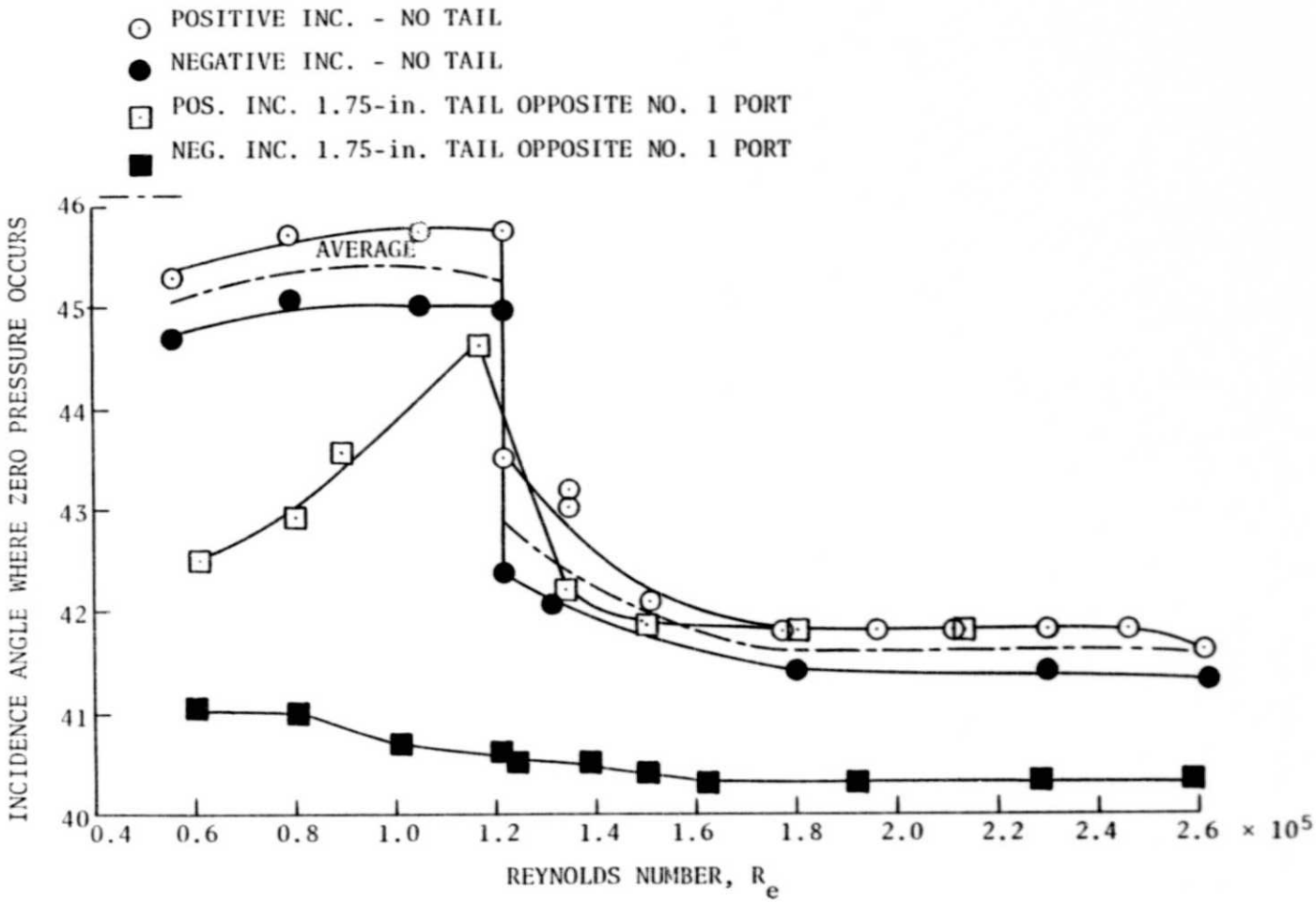

Figure 15. Variation of zero pressure point on the surface of the sphere with Reynolds number (tests in closed wind tunnel).

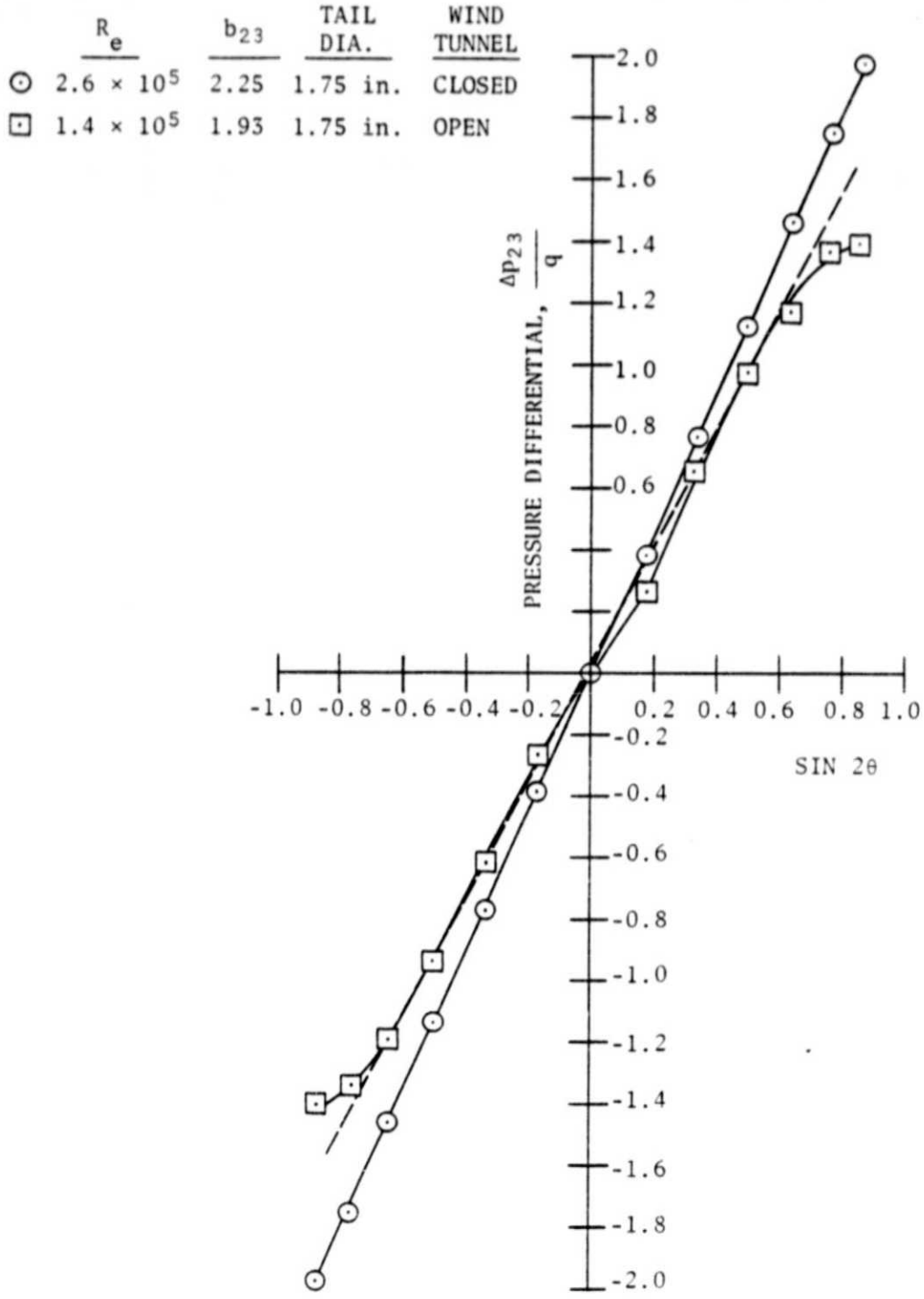

Figure 16. Variation of pressure differential $\Delta p_{23}/q$ with Reynolds number for the 2.5-in. sphere tested in the open and closed wind tunnels with tail attached.

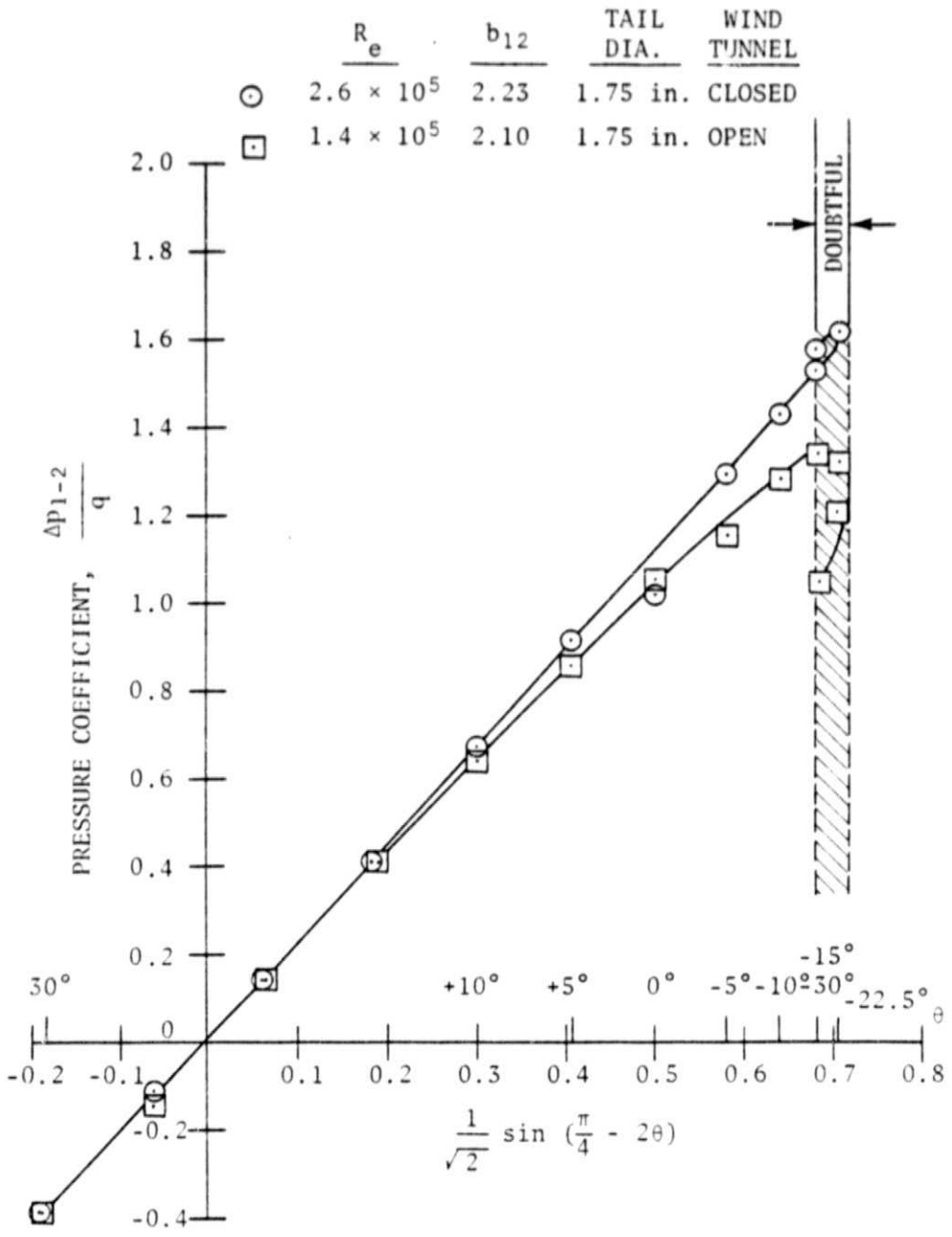

Figure 17. Variation of pressure differential $\Delta p_{12}/q$ with Reynolds number for the 2.5-in. sphere tested in the open and closed wind tunnels with tail attached.